IEEE Robotics and Automation Letters (RAL) paper presented at the
2020 IEEE/RSJ International Conference on Intelligent Robots and Systems (IROS)
October 25-29, 2020, Las Vegas, NV, USA (Virtual)

Development of Δ-type Mobile Robot driven by 3 Standing Wave Type Piezoelectric Ultrasonic Motors

J. Zhou, M. Suzuki, R. Takahashi, K. Tanabe, Y. Nishiyama, H. Sugiuchi, *Member, IEEE*, Y. Maeda, *Member, IEEE*, O. Fuchiwaki, *Member, IEEE*

Abstract— **Herein, we introduced a newly proposed mobile robot that uses three standing-wave type ultrasonic motors (USMs). The USM is composed of two stacked-type piezoelectric actuators. Recently, with the miniaturization of electronic and MEMS devices and the progress of the bio-medical science, the demand for multifunctional manipulation of those chip parts and bio-medical cells has increased. Conventional multiaxial stages are too bulky for the multifunctional manipulation where multiple manipulators are required. Conventional precise mobile robots are feasible for miniaturization of the multifunctional manipulation, although their cables influence the positioning repeatability. USMs are feasible actuators for realizing cableless robots because its energy efficiency is relatively higher than other motors with millimeter scale, although there is no article concerning the omnidirectional mobile robot using USMs thus far. The aim of this study is to develop a new type of the omnidirectional mobile robot driven by USMs. In experiments, we evaluated the feasibility by investigating velocity, positioning deviation, and achieving repeatability of translational movements under an open-loop control. Here, we determine the repeatability as a ratio of the standard deviation of the final points to the average path length. The proposed mobile robot achieves 18.6 to 31.4 mm/s of velocity and 4.1 to 9.1% of the repeatability with 200g weight.**

I. INTRODUCTION

Recently, with the miniaturization of electronic and MEMS devices and the progress of the bio-medical science, the demand for multifunctional manipulations of those chip parts and bio-medical cells has increased [1,2]. Conventional multiaxial stages are too bulky for the multifunctional manipulations where multiple manipulators are required [3].

In contrast, lightweight and compact self-propelling robots have been under development, such as those using omni wheels [4], driven by piezoelectric actuators [5, 6], shape memory alloys [7], and dielectric elastomers [8]. By mounting various tools on these robots and cooperating with each other, it is possible to achieve the compact multifunctional manipulations [9]. However, their speed decreases with the reduction in size, and their power supply is still relatively high.

In our previous work, an inchworm miniature robot using piezoelectric actuators and electromagnets was developed. The robot had advantages such as high positioning resolutions of 10 nm, lightweight of 100 g, and small size of 86 × 86 × 11 mm^3. Some practical applications of tiny sphere and bio-cell multi-functional manipulations have been demonstrated [10 -12].

However, it also has low speed of 7.3 mm/s and power consumption of 30 W. That power consumption has been still difficult to supply by non-contact power supply technologies [13,14]. Moreover, it is only able to drive on a well-polished ferromagnetic surface. These factors hinder its application.

Ultrasonic motors (USMs) are feasible actuators for overcoming these shortcomings because their energy efficiency is relatively higher than other motors with millimeter scale, although there is no article about the omnidirectional mobile robot using USMs thus far [15,16].

In this paper, we describe a newly-proposed mobile robot driven by three standing-wave type USMs, aiming at higher movement speed, lower power supply enough for cableless power supply, and movement on a non-magnetic surface.

In Section II, we explain the structure, driving principle, and fabrication of the robot. In Section III, we describe the modeling and input signals for the fabricated robot. In section IV, we evaluate the velocity and the positioning repeatability of the orthogonal movements of the robot with and without a load of 100 g/200 g. In section V, we summarize the achievements of this study and discuss the future works.

II. Δ-TYPE MOBILE ROBOT DRIVEN BY 3 USMS

Fig. 1 shows the newly proposed robot. It consists of a three standing-wave type linear USM (PI, P-661) (specification shown in TABLE I), an equilateral triangle shaped main stage, three sub-stages blocks, and three pairs of

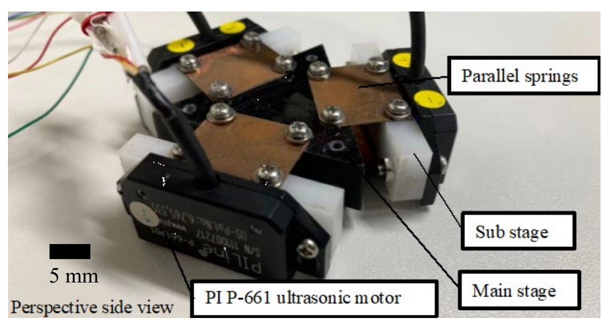

Figure 1. Perspective view of a Δ-type mobile robot driven by 3 USMs.

TABLE I SPECIFICATIONS OF PI P-661 ULTRASONIC MOTOR
(Detailed spec. is in supporting information (SI) in RA-L)

PHYSICAL QUANTITY	QUANTITY
Travel range	1.5 m (due to the length of frictional bar)
Resolution (open loop)	0.05 µm
Max. velocity	500 mm/s
Resonant frequency	210 kHz
Power source (DC)	12 V
Max. output Power	5 W
Mass	10 g
Dimensions	14 x 35 x 6 mm

The authors are with the Dept. of Mechanical Engineering, Yokohama National University (YNU), 79-5, Tokiwadai, Hodogaya-ku, Yokohama, Kanagawa, Japan (phone: +81-45-339-3693; e-mail: ohmif@ynu.ac.jp).

TABLE II COMPARISON OF SPECIFICATIONS AMONG PRECISE MOBILE ROBOTS
(Estimation methods of power are in SI in RA-L)

Physical quantity	**Proposed robot**	**Previous robot** [14]	**MiCRoN** [10]
Principle	Resonance drive	Inchworm	Stick slip
Max. speed [mm/s] (Power[W]) {Input voltage to PZT}	31.5 (4) {60Vpp, 210kHz, Sine}	7.3 (31) {120Vpp, 125Hz, Sine}	2 (No data) {400Vpp,1.5kHz, Sawtooth}
Resolution [μm]	0.05	0.01	0.002
Range [cm^2]	More than 50 x 50		
Repeatability [%] (Ratio of SD of final points to path length under open loop control)	3 – 15	2 – 3	No data
Mass [g]	45	100	12
Dimensions [mm^3]	55 × 55 ×14	86 × 86 × 11	12 x 12 x 17.5
Power [W] for 2 mm/s {Input voltage to PZT}	1 or less {60Vpp, 210kHz, sine, Duty ratio 7%}	29 {120Vpp, 33Hz, sine}	No data (400Vpp,1.5kHz, sawtooth)

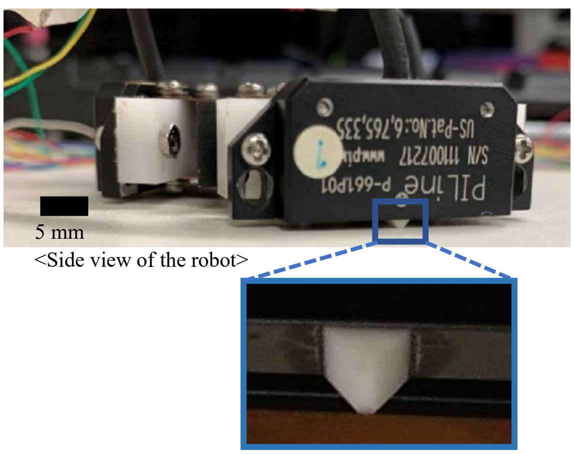

Figure 2. Close-up view of the friction tip from the bottom

parallel leaf springs. Each USM is fixed to its corresponding sub-stage, where its altitude can be adjusted. Each side of the main stage is linked to the 3 sub-stages through a pair of parallel leaf springs. Our design enabled the insertion of an additional tool in the main stage.

The specification of the proposed robot is compared with the conventional precise mobile robots in TABLE II. We also estimated their consumption energies for 2 mm/s in this table. We see that the proposed robot is much lower power required and also generates higher speed than the inchworm[14] and the stick-slip[10] based robots.

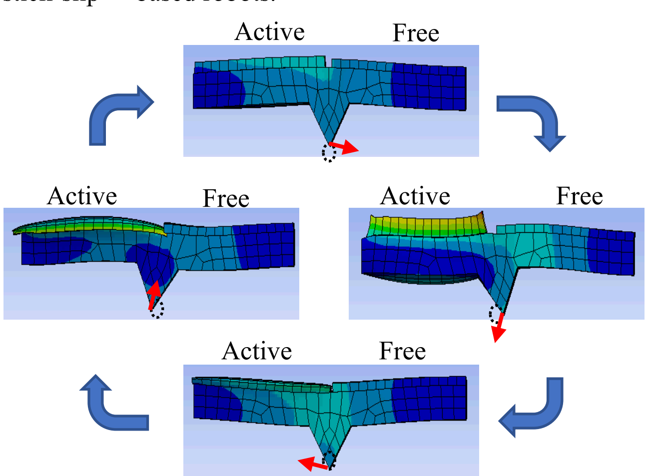

Figure 3. FEM results of the diagonal motions of the friction tip.

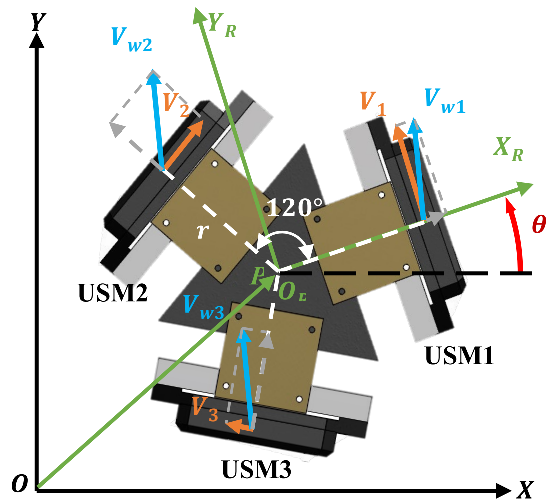

Figure 4. Kinematic model of Δ-type robot.

As shown in Fig. 2, the friction tips of the three USMs are designed to be in direct contact with the surface. When driving the robot, it needs to be placed on a smooth surface.

Figure 3 shows that one of the piezo elements inside the motor generates the standing wave vibration and the friction tips of the motors vibrate in an approximately diagonal manner. The friction tip scratches the surface and pushes the motor rightward. If the activated piezo element is switched to another, the tip pushes the motor leftward.

Each USM is controlled by an analog voltage from -10 V to +10 V input to the corresponding resonant circuit (C-184.161, PI), which generates the resonant frequency; the amplitude displacement and driving direction are adjusted by the analog input voltage.

As shown in Fig. 4, the frictional forces are oriented 120° from each other and have an offset *r* referring to the center of the robot. By properly changing the three input analog voltages, the composite vector of the three frictional force vectors can be oriented in any direction and simultaneously produce a moment for rotation on the surface; the robot can realize holonomic driving properties [6, 9-13].

III. KINEMATICS

Fig. 4 shows the kinematic model of the Δ-type mobile robot. We define the three USMs as USM1, USM2, and USM3 in counterclockwise direction. The center of the robot's frame is the center of mass of the robot. We determined that X_R, the axis of the robot frame, is perpendicular to the driving direction on USM1. θ denotes the orientation of the robot and is positive in the counterclockwise direction.

For each USM, its position respecting the robot frame can be described by multiplying the rotation matrix and the distance r from the center of the robot using the following equation:

$$P_i = \begin{bmatrix} x_i \\ y_i \end{bmatrix} = \boldsymbol{R}(\alpha_i) \cdot r \begin{bmatrix} 1 \\ 0 \end{bmatrix}$$

Where

$$\boldsymbol{R}(\theta) = \begin{bmatrix} \cos(\theta) & -\sin(\theta) \\ \sin(\theta) & \cos(\theta) \end{bmatrix}.$$

We can have

$$\boldsymbol{P_1} = r\begin{bmatrix}1\\0\end{bmatrix}, \boldsymbol{P_2} = \frac{1}{2}r\begin{bmatrix}-1\\\sqrt{3}\end{bmatrix}, \boldsymbol{P_3} = \frac{-1}{2}r\begin{bmatrix}1\\\sqrt{3}\end{bmatrix}. \quad (1)$$

The unit direction vector of the translation direction $\boldsymbol{D_i}$ of each USM is perpendicular to its position vector $\boldsymbol{P_i}$. Thus, it can be described as follows.

$$\boldsymbol{D_i} = \boldsymbol{R}\left(\frac{\boldsymbol{\pi}}{\boldsymbol{2}}\right)\frac{\boldsymbol{P_i}}{|\boldsymbol{P_i}|} = \frac{\boldsymbol{1}}{\boldsymbol{r}}\boldsymbol{R}\left(\frac{\boldsymbol{\pi}}{\boldsymbol{2}}\right)\boldsymbol{P_i}$$

It can be obtained that

$$\boldsymbol{D_1} = \begin{bmatrix}0\\1\end{bmatrix}, \boldsymbol{D_2} = \frac{1}{2}\begin{bmatrix}-\sqrt{3}\\1\end{bmatrix}, \boldsymbol{D_3} = \frac{1}{2}\begin{bmatrix}\sqrt{3}\\-1\end{bmatrix}. \quad (2)$$

According to the coordinate transformation equation, where $\boldsymbol{x}$ represents the coordination in world frame, $\boldsymbol{P}$ represents the coordination of the robot frame with respect to the world frame, $\boldsymbol{x}'$ denotes the coordination in the robot frame,

$$\boldsymbol{x} = \boldsymbol{p} + \boldsymbol{R}(\theta)\boldsymbol{x}' \quad (3)$$

the position of each USM can be derived from:

$$\boldsymbol{P_{wi}} = \boldsymbol{P} + \boldsymbol{R}(\theta)\boldsymbol{P_i}$$

and we can obtain them as follows:

$$\boldsymbol{P_{w1}} = \begin{bmatrix}x + r\cdot\cos(\theta)\\ y + r\cdot\sin(\theta)\end{bmatrix}, \boldsymbol{P_{w2}} = \begin{bmatrix}x + r\cdot\cos\left(\theta + \frac{2}{3}\pi\right)\\ y + r\cdot\sin\left(\theta + \frac{2}{3}\pi\right)\end{bmatrix}$$

$$\boldsymbol{P_{w3}} = \begin{bmatrix}x + r\cdot\cos\left(\theta + \frac{4}{3}\pi\right))\\ y + r\cdot\sin\left(\theta + \frac{4}{3}\pi\right)\end{bmatrix} \quad (4)$$

When we differentiate $\boldsymbol{P_{wi}}$ of the position of each USM in (4), we obtain $\boldsymbol{V_{wi}}$ of the velocity of $\boldsymbol{P_{wi}}$ with respect to the world frame, as given by

$$\boldsymbol{V_{wi}} = \dot{\boldsymbol{P}}_{\boldsymbol{wi}} = \dot{\boldsymbol{P}} + \dot{\boldsymbol{R}}(\boldsymbol{\theta})\boldsymbol{P_i} \quad (5)$$

$\boldsymbol{V_{wi}}$ is the sum of the translational velocity and the velocity determined by the rotational motion. Substituting (1) into (5), $\boldsymbol{V_{wi}}$ can be obtained as follows:

$$\boldsymbol{V_{w1}} = \begin{bmatrix}\dot{x} - r\cdot\dot{\theta}\sin(\theta)\\ \dot{y} + r\cdot\dot{\theta}\cos(\theta)\end{bmatrix}, \boldsymbol{V_{w2}} = \begin{bmatrix}\dot{x} - r\cdot\dot{\theta}\sin\left(\theta + \frac{2}{3}\pi\right)\\ \dot{y} + r\cdot\dot{\theta}\cos\left(\theta + \frac{2}{3}\pi\right)\end{bmatrix},$$

$$\boldsymbol{V_{w3}} = \begin{bmatrix}\dot{x} - r\cdot\dot{\theta}\sin\left(\theta + \frac{4}{3}\pi\right)\\ \dot{y} + r\cdot\dot{\theta}cos\left(\theta + \frac{4}{3}\pi\right)\end{bmatrix} \quad (6)$$

Although USMs should generate the velocity in any direction equal to $\boldsymbol{V_{wi}}$, they generate the velocity in a constant direction with respect to the robot frame. Here, we approximate that their generated velocities are equal to the inner product of the unique direction and the translation direction of the robot.

In other words, we approximate that the USMs generate frictional force only in the driving direction because the frictional force in the perpendicular direction should be minimized so as not to generate unexpected vibrations and positioning errors. We investigate the modeling error of this approximation of the anisotropic friction in the next section.

By applying the estimation mentioned above, the translational velocities of the USMs with respect to the robot frame can then be obtained from the following equation:

$$\boldsymbol{V_i} = \boldsymbol{V_{wi}}^T\cdot(\boldsymbol{R}(\theta)\boldsymbol{D_i}) \quad (7)$$

By substituting (6) into equation (7), each USM's translational velocity can be obtained:

$$\begin{bmatrix}V_1\\V_2\\V_3\end{bmatrix} = \begin{bmatrix}-\sin(\theta) & \cos(\theta) & r\\ \sin\left(\theta - \frac{\pi}{3}\right) & -\cos\left(\theta - \frac{\pi}{3}\right) & r\\ \sin\left(\theta + \frac{\pi}{3}\right) & -\cos\left(\theta + \frac{\pi}{3}\right) & r\end{bmatrix}\cdot\begin{bmatrix}\dot{x}\\\dot{y}\\\dot{\theta}\end{bmatrix} \quad (8)$$

where $\dot{x}, \dot{y}, and\ \dot{\theta}$ represent the translational and rotation angular speeds of the robot mass center, respectively, with respect to the world frame.

By applying the inverse matrix, we represent the robot's 3 axes velocity, $\dot{x}, \dot{y}, and\ \dot{\theta}$, by the 3 velocities of the USMs, $V_1, V_2, and\ V_3$, as given by

$$\begin{bmatrix}\dot{x}\\\dot{y}\\\dot{\theta}\end{bmatrix} = \begin{bmatrix}\frac{-2}{3}\sin(\theta) & \frac{-2}{3}\sin\left(\frac{\pi}{3} - \theta\right) & \frac{2}{3}\sin\left(\frac{\pi}{3} + \theta\right)\\ \frac{2}{3}\cos(\theta) & \frac{-2}{3}\cos\left(\frac{\pi}{3} - \theta\right) & \frac{-2}{3}\cos\left(\frac{\pi}{3} + \theta\right)\\ \frac{1}{3r} & \frac{1}{3r} & \frac{1}{3r}\end{bmatrix}\begin{bmatrix}V_1\\V_2\\V_3\end{bmatrix}. \quad (9)$$

Because the resonant frequency of each USM is a unique value and the amplitude displacements are adjusted by the corresponding analog input voltages, the USMs' velocity of $V_1, V_2, and\ V_3$ is also adjustable by the input voltages from -10 V to 10 V. We determined the theoretical ratio of the input analog voltages from the ratio of $V_1, V_2, and\ V_3$ from (9) in the experiments with their maximum input voltages of 5 V as explained in section S5 in supporting information in RA-L.

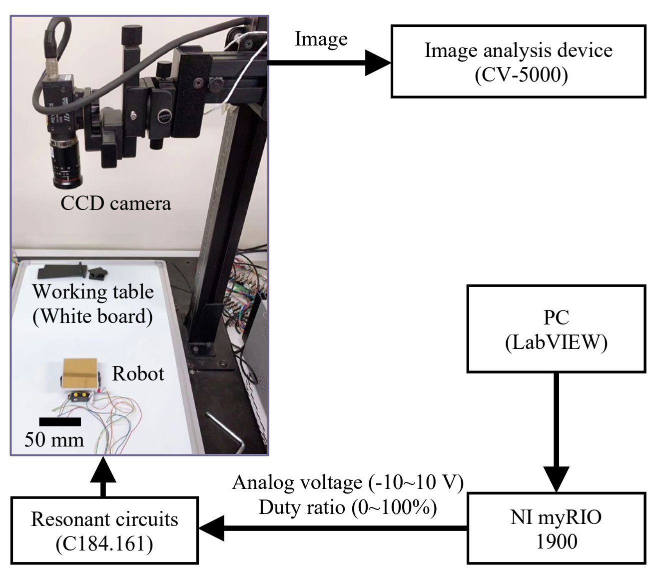

Figure 5. Experimental setup.

IV. EXPERIMENTS

To test the positioning property of the newly developed Δ-type robot, an open-loop control experiment was conducted. An image analysis system, as shown in Fig. 5, was used to record the track of the robot. This system is composed of a low-distortion lens (CA-LHR8, Keyence), a digital CCD camera (CV-H500M, Keyence), an image analysis device (CV-5000, Keyence), a portable reconfigurable I/O device (NI, myRIO-1900), and a personal computer with LabVIEW. We chose a commercially available whiteboard after trying various materials and roughness for the ground surface. One of the main purposes of this paper is investigating the range of the repeatability of the proposed mobile robot on the reasonable floor for expanding the applications. The coefficient of static and kinematic frictions between the board and the robot is measured as 0.17 ± 0.2 and 0.072 ± 0.004 (average ± SD) respectively by the inclined surface method (as shown in tables S3 and S4-2 in supporting information (SI) in RA-L). We confirmed that the USMs were vibrating slightly by an electromagnetic noise even when the control voltage was 0V (in tables S5-1, S5-2, and S5-3 in RA-L). The electromagnetic noise was affected the USMs because we cut the shield cables for decreasing the cables' tensions.

We supposed that the very low kinematic friction under the condition of the slight vibration is one of the main reasons why the robot realizes omnidirectional mobility.

The experiment was separated into a weight-loaded group and a load-free group. The steps of the experiment are as follows:

1) Load the weight on the robot;
2) Adjust the robot's location and attitude angle;
3) Manually adjust the theoretical ratio of the input voltages until the movement direction of the robot is close to the target direction (SI in RA-L);
4) Move the robot for 10 s by measuring the track using the image analysis device;
5) Repeat 10 times from Step 4;
6) Repeat from step 2 for each movement (12 translations and 2 rotations for a load free and 4 translations for weighted groups respectively;
7) Calculate the repeatability from the obtained data.

In this paper, we determine the repeatability as a ratio of the standard deviation of the final points to the average path length. The experimental conditions are shown in Table III. We define ϕ as moving direction of the translational motions.

TABLE III EXPERIMENTAL CONDITIONS

Working table	White board
Initial attitude angle of the robot	$\theta = 0$
Duration per track	5 s
Measuring frequency	10 Hz
Search range of camera	2413 x 2049 pixels
Pixels per mm	8.9 pixels/mm
Recorded tracks per direction	10 tracks
Movements for a load free group	12 translational directions (ϕ =0~330º in 30º scale), 2 rotations (CW, CCW)
Movements for load weighted groups	4 translational directions (ϕ =0º, 90º, 180º, 270º)

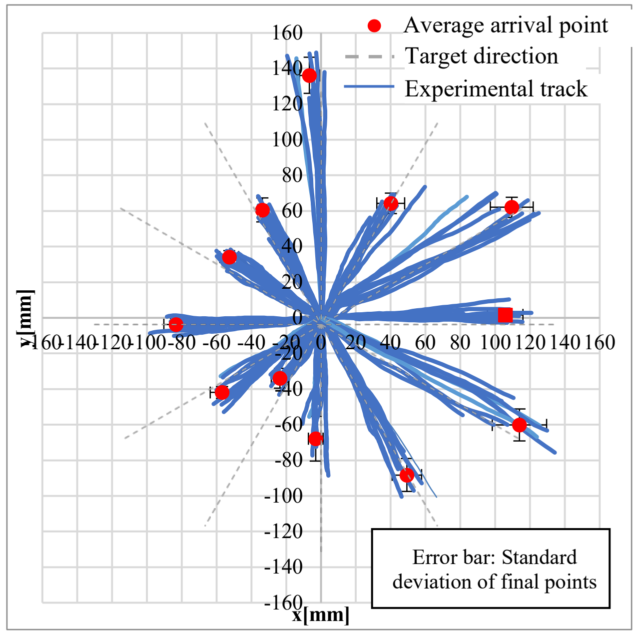

Figure 6. Trajectories of translational movements with no weight.

V. EXPERIMENT RESULTS

A. Translational movement of the load-free group

Fig. 6 shows the tracks of translational movements. The blue dotted lines show the 12 directions. The red points are the average arrival points of each direction. The deviation bars represent the corresponding standard deviations in the x and y axes of the average arrival points.

We found that the translational tracks significantly deviate from their target directions. The standard deviation of the distances from the final to the average arrival points is distributed from 6 to 17 mm. We considered that the distribution is mainly caused by a nonuniformity of the number of frictional tips contacting to the floor simultaneously (we discuss in S6 of SI in RA-L), the tension of the cables and the nonuniformity of the frictional condition of the working surface that affects especially the fluctuation of the attitude angle θ.

B. Rotational motion of the load-free group

Figs. 7 and 8 show the rotational tracks of an offset mark on the robot in CW and CCW, respectively. Blue lines are tracks. The red points represent the ideal rotation centers. Brown points represent average centers. Deviation bars show the standard deviation of the experimental rotation centers (blue points) from the average rotation center.

The average rotation speed reached 144°/s. The standard deviation of the rotation centers to the average rotation center was 3.9 mm in CCW and 4.3 mm in CW. The circles of rotation were also not properly closed. We consider that the unevenness of the frictional condition and cable tension may be responsible for this.

C. Translational motion of the loaded group

The Δ-type robot is designed to work by applying manipulators. It is necessary to investigate the positioning property when it is loaded with additional weight.

Fig. 9 shows the image of the Δ-type robot loaded with a weight. We moved the robot with two different weights of 100 g and 200 g, whose tracks are shown in Figs. 10 and 11,

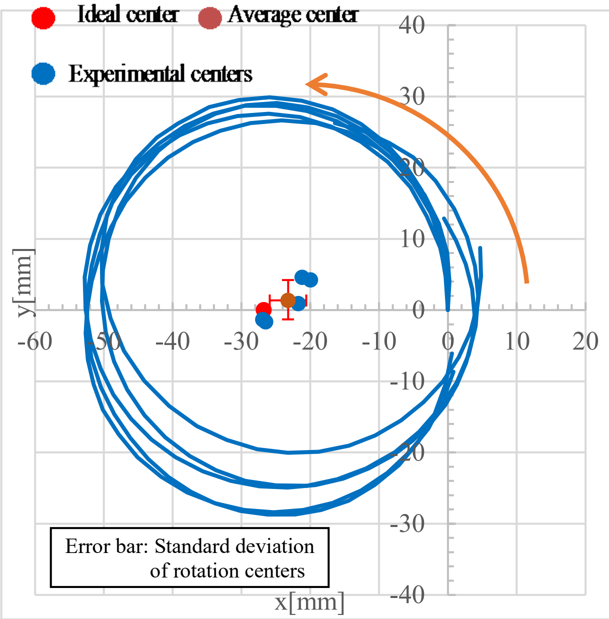

Figure 7. Trajectories of rotation in CCW with no weight.

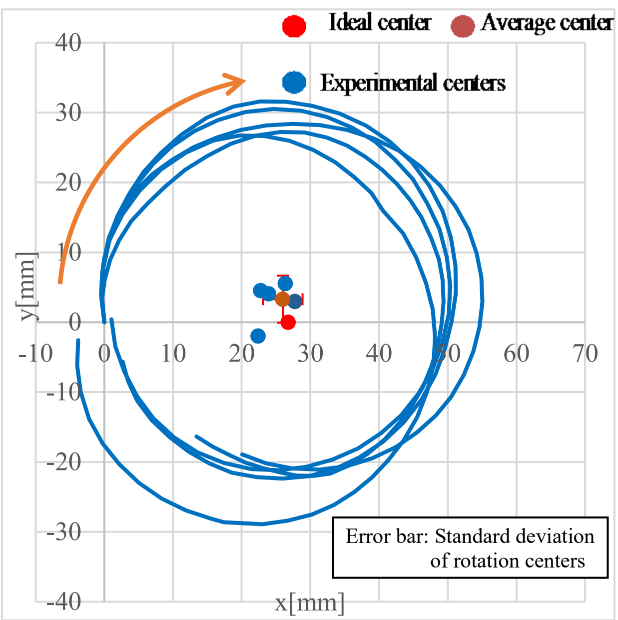

Figure 8. Trajectories of rotation in CW with no weight.

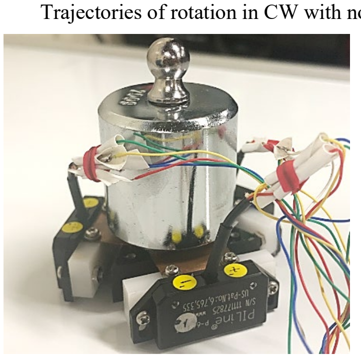

Figure 9. Δ-type robot mounted with a weight

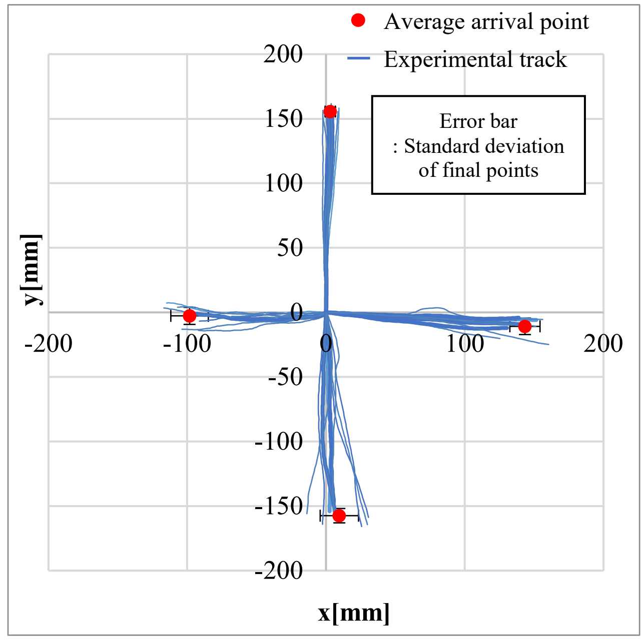

Figure 10. Tracks with 100 g weight in orthogonal directions.

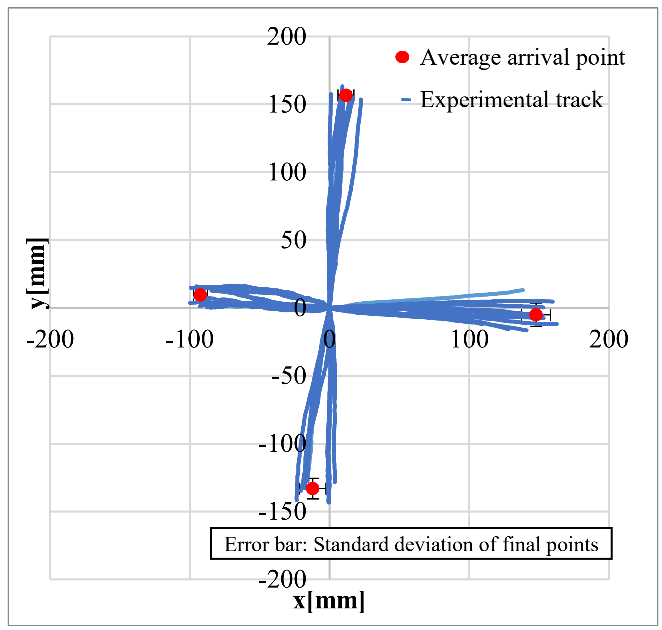

Figure 11. Tracks with 200 g weight in orthogonal directions.

respectively. The blue lines show the tracks of 4 orthogonal directions. The red points are the average arrival points of each direction. The deviation bars represent final arrival points' standard deviation in x and y axes from the average arrival points. The standard deviation in the 100 g group ranged from 4 to 15 mm, and in the 200 g group was from 6 to 12 mm.

D. Comparison of positioning properties

Fig. 12 shows the comparison of average track lengths of the three groups in 4 directions. It can be observed that in all four directions, the robot ran a distance 20 mm longer when it was loaded with weight in the same time period. Especially,

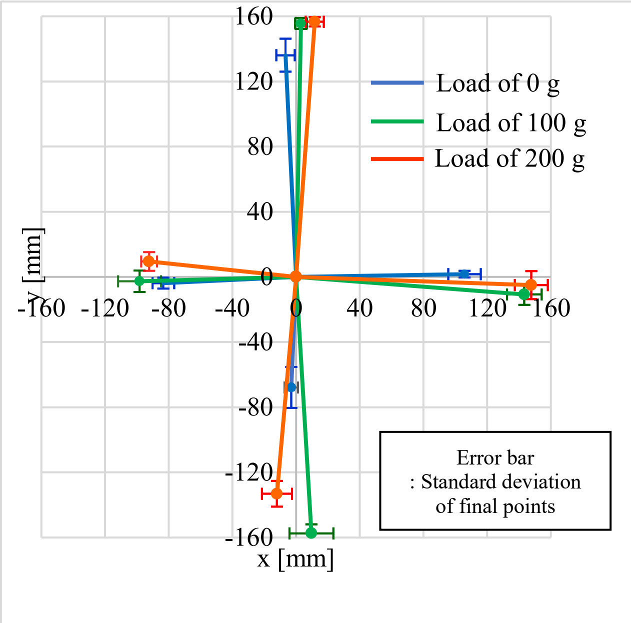

Figure 12. Comparison of average track lengths and deviations of the final points among loads of 0 g, 100 g, and 200 g.

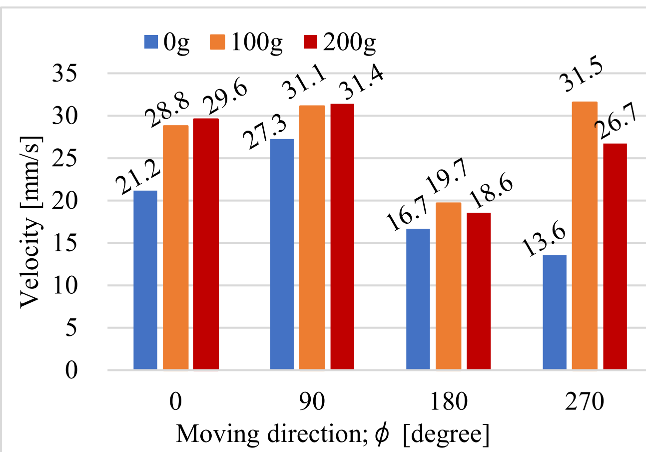

Figure 13. Comparison of velocities in 4 directions with 0, 100, and 200 g.

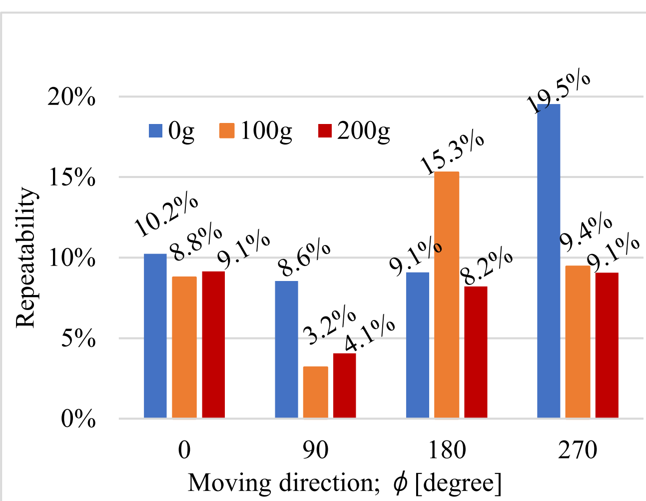

Figure 14. Comparison of the repeatabilities in 4 directions with 0, 100, and 200 g. (The repeatability is determined as a ratio of the standard deviation of the final points to the average path length.)

in -x direction, when the robot was loaded with weight, the distance became more than twice that of the non-weight group.

Fig. 13 depicts the differences in velocities among the conditions tested. The velocities are increased by 2–18 mm/s when loaded with weight. A reasonable amount of weight increases the velocity because the frictional conditions between each frictional tip and the working surface improve.

We consider that the difference of the average final points among those experiments is caused by their systematic errors due to the wire tension and the difference of load distribution among the 3 friction tips.

Fig. 14 shows the comparison of the repeatabilities among the three groups. The repeatability is basically 2%–10% better in the groups with weight loading. This is because the weight provides the friction tips of the motors a better contact with the working surface and reduced slips during the movement.

VI. Conclusion and Future Prospects

In this research, we constructed a prototype robot using standing wave type USMs. In a load-free experiment, the robot realized omnidirectional movement on a non-magnetic surface. It reached a maximum translational speed of 27.3 mm/s. The positioning repeatability was distributed from 8.6 to 19.5%. Large deviations and low repeatability are considered mainly due to the nonuniformity of the number of frictional tips contacting to the floor simultaneously, the tension of the cables, and the nonuniformity of the frictional condition of the working surface. Those factors affect especially the fluctuation of the attitude angle θ.

In comparison experiments, we found that by loading a reasonable weight of 100g on the robot, the speed could be improved up to 31.5 mm/s from 13.6 mm/s. We also confirmed that the repeatability is distributed from 4.1 to 9.1% with 200g weight. This means that the proposed robot is feasible for efficient manipulations and positions with 200 g of manipulators.

In future works, we plan to increase the number of the friction tip for improving the repeatability as explained S6 in SI in RA-L. We also plan to realize motion compensation and feedback control, which improve the precision and repeatability of the robot, and it is necessary for applications requiring automatic control. We also plan to introduce cableless technology. It improves the compactness and repeatability of the robot because it is no longer affected by cable tension. Furthermore, we plan to conduct experiments to check the effect of decreasing the surface roughness and the flatness error on the repeatability because it is also considered to be responsible for deviation. Finally, we plan to measure the positioning properties in sub-micrometer scale with a XYθ position sensor organized by four encoders[17]. We also develop a servo control method with sub-micrometer resolution to test its ability for precise operations. Feasible applications of the proposed robot are chip parts assembling, bio-medical applications, and wide area flexible positioning of lightweight tools, sensors, and manipulators where versatility and cableless is required.

REFERENCES

[1] W. Hagiwara, T. Ito, K. Tanaka, R. Tokui, and O. Fuchiwaki, “Capillary Force Gripper for Complex-Shaped Micro-Objects with Fast Droplet Forming by On-Off Control of a Piston Slider,” *RA-L*, Vol. 4, No. 4, pp. 3695–3702, Jul 2019, doi: 10.1109/LRA.2019.2927939.

[2] T. Chen, L. Sun, L. Chen, W. Rong and X. Li, “A hybrid-type electrostatically driven microgripper with an integrated vacuum tool,” *Sensors and Actuators A*, vol. 158, pp. 320–327, Mar 2010, doi: 10.1016/j.sna.2010.01.001

[3] H. Xie and S. Régnier, "Development of a Flexible Robotic System for Multiscale Applications of Micro/Nanoscale Manipulation and Assembly," *TMech*, vol. 16, no. 2, pp. 266-276, April 2011, doi: 10.1109/TMECH.2010.2040483

[4] F. Tajti, G. Szyayer, B. Kovacs and P. Korondi, “Robot base with holonomic drive,” *Proc. of IFAC*, vol. 47, No. 3, pp. 5715–5720, Aug 2014, doi: 10.3182/20140824-6-ZA-1003.00785

[5] N. A. Saadabad h. Moradi and G. Vossoughi, “Dynamic modeling, optimized design, and fabrication of a 2DOF piezo-actuated stick-slip mobile microrobot,” *Mechanism and Machine Theory*, vol. 133, pp. 514–530, Mar 2019, doi: 10.1016/j.mechmachtheory.2018.11.025

[6] S. M. Martel, C. O. Lorenzo, B. C. F. Juan, R. Stefen, K. Torsen and S. Jeremy, “General description of the wireless miniature NanoWalker robot designed for atomic-scale operations,” *Proc. of SPIE*, vol. 4568, pp. 231–240, Oct 2001, doi: org/10.1117/12.444130

[7] X. Huang, K. Kumar, M. K. Jawed, A. M. Nasab, Z. Y. W. Shan and C. Majidi, “Chasing biomimetic locomotion speeds: Creating untethered soft robots with shape memory alloy actuators,” *Sci. Robot*. vol. 3, no.25, eaau7557, Dec 2018, doi: 10.1126/scirobotics.aau7557

[8] X. Ji. X. Liu, V. Cacucciolo, M. Imboden, Y. Civet, A. E. Haitami, S. Cantin, Y. Perriard and H. Shea, “An autonomous untethered fast soft robotic insect driven by low-voltage dielectric elastomer actuators,” *Sci. Robot*. Vol. 4, No. 37, eaaz6451, Dec 2019, doi: 10.1126/scirobotics.aaz6451

[9] S. Fatikow, “Automated Nanohandling by microrobots, Springer series in advanced manufacturing,” ISBN 978-1-84628-977-4, 2008

[10] W. Driesen, T. Varidel, S. R. egnier, and J-M Breguet, Micro manipulation by adhesion with two collaborating mobile micro robots, J. Micromech. Microeng, Vol. 15, S259–S267, Sep 2005, doi: 10.1088/0960-1317/15/10/S02

[11] O. Fuchiwaki, Y. Tanaka and T. Hyakutake, “Multi-axial non-contact in situ micromanipulation by steady streaming around two oscillating cylinders on holonomic miniature robots”, *MANO,* Vol. 22, No. 80, July 2018. doi: org/10.1007/s10404-018-2098-5

[12] O. Fuchiwaki, A. Ito, D. Misaki, H. Aoyama, “Multi-axial Micromanipulation Organized by Versatile Micro Robots and Micro Tweezers,” *Proc. of ICRA 2008*, pp. 893–898, Jun 2008, DOI: 10.1109/ROBOT.2008.4543318

[13] O. Fuchiwaki, Insect-sized holonomic robots for precise, omnidirectional, and flexible microscopic processing, PE, vol. 37, no. 1, pp. 88–106, Jan 2013, doi: 10.1109/IROS.2015.7353561

[14] O. Fuchiwaki, M. Yatsurugi, and T. Sato, The basic performance of a miniature omnidirectional 6-legged inchworm robot from cm- to μm-scale precise positioning, TMRSJ, Vol. 39, No. 2, pp. 211-215, Jan 2014, doi: 10.14723/tmrsj.39.211

[15] K. Takemura, Y. Ohno, and T. Maeno, Design of a Plate Type Multi-DOF Ultrasonic Motor and Its Self-Oscillation Driving Circuit, TMECH, Vol. 9, No. 3, pp. 474-480, Sep 2004, doi: 10.1109/TMECH.2004.834643

[16] Y. Liu, J. Yan, L. Wang, W. Chen, A Two-DOF Ultrasonic Motor Using a Longitudinal–Bending Hybrid Sandwich Transducer, IEEE TRANSACTIONS ON INDUSTRIAL ELECTRONICS, Vol. 66, No. 4, pp. 3041-3050, Apr 2019, doi: 10.1109/TIE.2018.2847655

[17] O. Fuchiwaki, M. Yatsurugi, A. Ogawa, Design of an integrated 3DoF inner position sensor and 2DoF feedforward control for a 3DoF precision inchworm mechanism, Proc. of ICRA 2013, pp. 5475–5481, May 2013, doi: 10.1109/ICRA.2013.6631365